Theoretical and Applied Mechanics Letters 14 (2024) 100510

Contents lists available at ScienceDirect

Theoretical and Applied Mechanics Letters

journal homepage: www.elsevier.com/locate/taml

A study of the effect of local scour on the flow field near the spur dike

Yu-Tian Li[a,b], Jie-Min Zhan[b,*], Wing-Hong Onyx Wai[c]

[a] Department of Industrial Design, School of Industrial Design and Ceramic Art, Foshan University, Foshan 528000, China
[b] Department of Applied Mechanics and Engineering, Shenzhen Campus of Sun Yat-sen University, Shenzhen 518107, China
[c] Department of Civil and Environmental Engineering, The Hong Kong Polytechnic University, Hong Kong 999077, China

ARTICLE INFO

Keywords:
Spur dike
Local scour
Large eddy simulation
Down flow
Horseshoe vortex system

ABSTRACT

The flow field near a spur dike such as down flow and horseshoe vortex system (HVS) are susceptible to the topographic changes in the local scouring process, resulting in variation of the sediment transport with time. In this study, large eddy simulations with fixed-bed at different scouring stages were conducted to investigate the changes in flow field. The results imply that the bed deformation leads to an increase in flow rate per unit area, which represent the capability of sediment transportation by water, in the scour hole. Moreover, the intensity of turbulent kinetic energy and bimodal motion near the sand bed induced by the HVS were also varied. However, the peak moments between the two sediment transport mechanisms were different. Hence, understanding the complex feedback mechanism between topography and flow field is essential for the local scour problem.

Spur dike is a widely used hydraulic structure in river training projects, which can protect riverbanks, maintain the channel depth and promote the diversity of the aquatic environment by the deflection and contraction to the incoming flow [1–2]. However, the complex hydraulic dynamics and local scour phenomenon brought by the construction of the spur dike affect the stability of the structure itself, which may cause damage at excessive scour depth[3]. Therefore, lots of researchers had conducted experimental and numerical studies on the local scour problem near the spur dike[4,5] to find the main factors which contribute to the sediment transport. In general, the increased flow rate per unit width, the down flow in front of the spur dike and the horseshoe vortex system (HVS) are the three main factors prompting the scour. Among these, the narrowing of the river channel by the spur dike increases the flow velocity near the head, which implies that the increase in scour capacity by the water flow, is the direct factor that initiates local scour. Meanwhile, some of the blocked water was diverted to rush the riverbed, known as the down flow. Unlike the general sediment transport, which is caused by the shear stress between the two layers of water and sand, down flow could agitate the sand layer by direct collision between the water and the sediment. As for the HVS, it could enhance the sand transport capacity of the water by inducing complex vortex-flow in the near-bed region[6,7]. And the mechanism is the internal turbulence intensity in the vortex-flow was higher than the surroundings which is capable of pushing the sediment particles due to the strong turbulent stresses at the bed surface[8–10].

In general, local scour is a complex phenomenon formed under the combined action of several main flow patterns. The flow field and the topography are closely related, so the deforming river bed forced the flow to change accordingly until a dynamic equilibrium between the water and the bed was reached. Biron et al. [4], in their study of the three-dimensional flow structure near the spur dike, pointed out that understanding the interaction mechanism between topography and hydrodynamic properties is extremely important for understanding the local scour problem. However, there is a lack of studies on the evolutionary patterns of the main flow structures causing scour during topographic changes and their effects on sand transport over time. Unger et al. [11] and Guan et al. [12] conducted experimental studies on the evolution of the HVS during the development of the scour hole. The results show that the primary vortex of the HVS temporarily disappeared during the initial scouring stage of rapid topographic change due to the deflection of the down flow. According to the experimental results of jet scouring, Si et al. [13] pointed out that there is a special stage during local scouring process in which the mean turbulent kinetic energy of the main vortex in the flow field was weakened to the smallest value and then gradually recovered with the further enlargement of the scour hole. All of the above studies suggest that there is a significant effect of topographic changes on the original flow field. And the main flow structure may have undergone a phase when the strength or energy of the flow reached the peak value before the scour reached the equilibrium state.

Numerical techniques that can capture the dynamics of the three-dimensional flow have been used by Koken et al. [10] to understand the mechanism of sediment transport near an in-stream structure with the imposed scour hole obtained from experiment. Their results show that

* Corresponding author.
E-mail address: stszjm@mail.sysu.edu.cn (Jie-Min Zhan).

https://doi.org/10.1016/j.taml.2024.100510
Received 15 December 2023; Received in revised form 1 March 2024; Accepted 2 March 2024
Available online 6 March 2024
2095-0349/© 2024 The Author(s). Published by Elsevier Ltd on behalf of The Chinese Society of Theoretical and Applied Mechanics. This is an open access article under the CC BY-NC-ND license (http://creativecommons.org/licenses/by-nc-nd/4.0/)

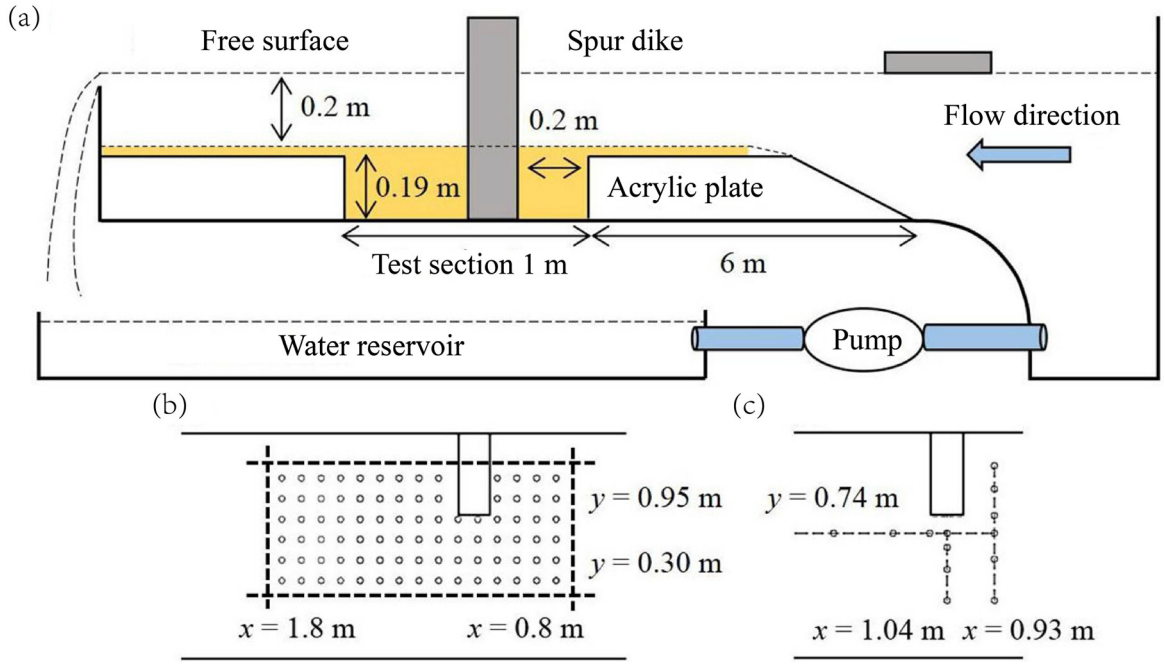

Fig. 1. (a) Schematic diagram of the recirculation flume. (b) Topographic measurement range. (c) Flow velocity measurement cross section.

numerical calculations based on experimental topography can provide more realistic and accurate flow field data. This makes it possible to visualize the HVS and characterize their shapes and positions relative to the bed. In this study, the scoured bed in the initial and equilibrium stages of a non-emerged single spur dike was investigated experimentally. Then the corresponding fixed bed large eddy simulations were completed using the measured topographic data. Finally, the evolution of the flow field near the spur dike during the local scouring process were compared based on the numerical results. And the dynamic characteristics of the major flow structures, such as the down flow and HVS, were analyzed.

The clear water scouring experiments were carried out in a 13 m long by 1 m wide glass flume, as shown in Fig. 1(a), at Sun Yat-sen University. The circulation system used for the continuous scouring consists of the flume, a water reservoir and four inverter pumps. Curved deflector and wave suppressor are installed at the inlet to create a stable outflow. Four variable frequency controllers are used to regulate the pump to achieve the target flow rate and the end of the flume is fitted with an adjustable gate to control the water depth. A 10 m long guide rail is installed next to the flume and a sliding platform could move the measuring instruments through the rail to the designated location. The scour test section was located 6 m downstream of the inlet and was 1 m long with a sand layer of 0.2 m thickness. The rest area within the flume was padded at the bottom using an acrylic sheet to a height of 0.19 m. Then a 0.01 m thick layer of sand was placed on the surface of the sheet so that it was flush with the surface of the sand layer in the test section. A non-emerged rectangular vertical spur dike was placed 0.2 m downstream of the start position of the test section, and the structure was 0.08 m wide in the direction of the incoming flow and 0.2 m long in the transversal direction.

All the cases in the experiment had the same incoming velocity U and water depth d, differing only in the scouring time, as shown in Table 1. The Reynolds numbers (Re) based on U and d were 30,500. At the start of the scouring, the soft start program of the variable frequency converter gradually increased the flow rate from zero to the target value within 30 s. When a pre-set scouring time was reached, the pumps were gradually switched off using the same program. Finally, the water in the recirculating flume was slowly pumped out by another small pump to expose the sand bed to the air. An infrared detector was then used to measure the elevation of the bed in the designated area as shown in Fig. 1(b). In addition, in Case C4, the velocity distribution in some areas was measured using an acoustic doppler velocity meter (ADV) 3 h before the end of the scouring for the numerical simulation, which consists of the vertical flow velocity profiles at 1 m upstream of the spur dike and at each of the gaging points in Fig. 1(c).

Table 1
Experimental conditions.

Case	U_0 (m·s^{-1})	d (m)	Re	T (min)
C1	0.155	0.2	3.1×10^4	30
C2	0.155	0.2	3.1×10^4	80
C3	0.155	0.2	3.1×10^4	150
C4	0.155	0.2	3.1×10^4	3000

Transient three-dimensional flow was prevalent in the vicinity of in-stream structures, and bed deformation due to local scouring further complicated the flow field. The comprehensive flow field data obtained by numerical simulation provides a new insight into such a problem, as opposed to experimental studies where only a limited number of measurement points can be measured. Among the commonly used numerical methods, LES is suitable for computing unsteady and complex flows at high Reynolds numbers by filtering the eddy structure below the size threshold. Therefore, this study is based on ANSYS Fluent 15.0 software using LES to calculate the three dimensional flow field in the vicinity of spur dike under fixed bed conditions.

The governing equations obtained after filtering the N-S equations using the filter function are:

$$\frac{\partial \rho}{\partial t} + \frac{\partial (\rho \overline{u_i})}{\partial x_i} = 0, \tag{1}$$

$$\frac{\partial \overline{u_i}}{\partial t} + \frac{\partial}{\partial x_j}(\overline{u_i u_j}) = -\frac{1}{\rho}\frac{\partial \overline{p}}{\partial x_i} + f_i + \frac{\partial}{\partial x_j}\left[\nu\left(\frac{\partial \overline{u_i}}{\partial x_j} + \frac{\partial \overline{u_j}}{\partial x_i}\right) + \tau_{ij}\right], \tag{2}$$

where $x_i, x_j (i, j = 1, 2, 3)$ are the Cartesian coordinates; $\overline{u_i}, \overline{u_j} (i, j = 1, 2, 3)$ are the filtered velocity components; $\overline{p}$ is the filtered pressure; f_i is the volumetric force component; ν represents the kinematic viscous coefficient of the fluid molecules; and τ_{ij} represents the sublattice Reynolds stress, which is the effect of vortices smaller than the grid size in the sub

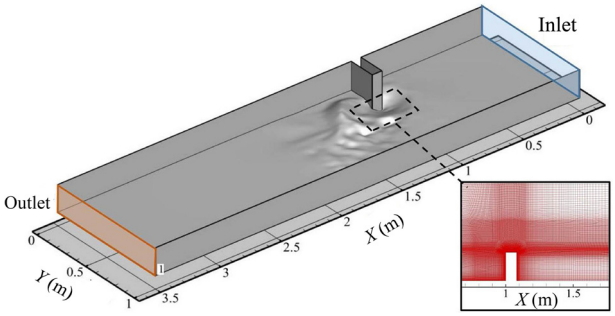

Fig. 2. Schematic diagram of the computational domain and grid.

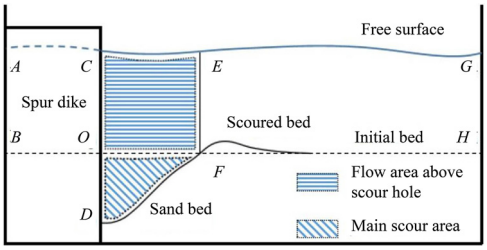

Fig. 4. Schematic diagram of scour hole zoning.

grid model. In this study, the Smagorinsky sublattice model proposed by Lilly [14] is used to close the governing equations, which is based on the assumption of isotropic vortex viscosity, so the subgrid Reynolds stress can be written as:

$$\tau_{ij} = -2\nu_t \overline{S_{ij}} + \frac{1}{3}\tau_{kk}\delta_{ij}, k = 1, 2, 3, \tag{3}$$

$$\nu_t = (C_s \Delta)^2 \left|\overline{S_{ij}}\right|, \tag{4}$$

$$\overline{S_{ij}} = \frac{1}{2}\left(\frac{\partial \overline{u_i}}{\partial x_j} + \frac{\partial \overline{u_j}}{\partial x_i}\right), \tag{5}$$

where ν_t represents the turbulent eddy-viscosity coefficient, C_s is the Smagorinsky coefficient, $\triangle$ is the size of the filter lattice, and $\overline{S_{ij}}$ is the filter strain tensor.

The above governing equations are discretized using the finite volume method where the spatial discretization uses finite center differences and the time term uses first order implicit discretization. The system of equations is solved using the SIMPLE method with pressure and velocity coupling.

The same scale numerical computational domain shown in Fig. 2 is established based on the above scouring experiments. The length of the numerical flume was taken as 3.5 m, and the scatter data of the bed elevation measured in the experiments were used to reconstruct the bottom boundary of the computational domain by interpolation (Fig. 2 shows an example of the reconstructed bed surface of C4). Two sets of coarse and fine grids are used in the numerical calculations to verify the grid independence and reliability of the numerical model, with the total number of coarse and fine grids being 8 million (grid I) and 10 million (grid II) respectively. The main difference between the two sets of grids is that the grid size in the vicinity of spur dike is 2.5 cm in the coarse grid and 1.6 cm in the fine grid. The areas close to the wall in both sets of grids were adapted, and the average $Y+$ of the first cells near the wall was approximately 0.8.

The inlet boundary of the computational domain was set as a velocity inlet and the velocity profile was given by fitting the ADV measurements 1 m upstream of spur dike in the C4 case with an average turbulence of 8%. The outlet boundary was set as a pressure outlet and the water level at the outlet was controlled according to the water depth measured in experiment(d = 0.2 m). No-slip boundary conditions were used at the bottom and both side walls.

The comparison results in Fig. 3 show that the numerical results of both grid sets in the region near the spur dike are in good agreement

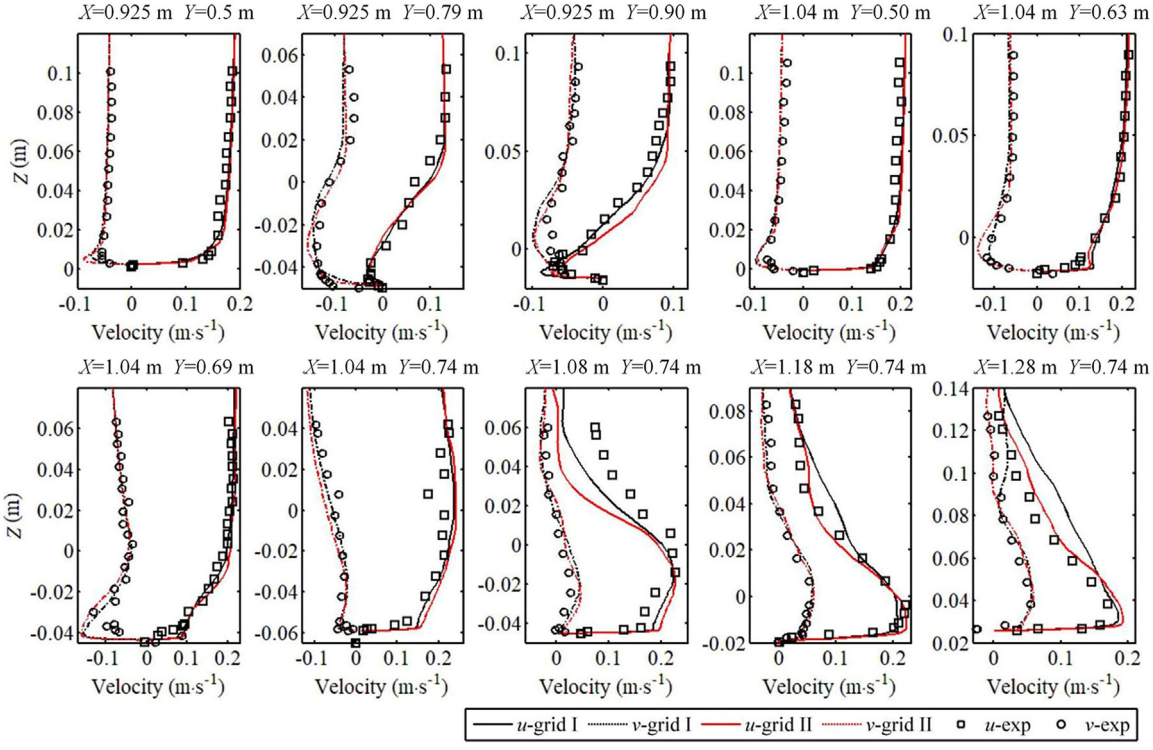

Fig. 3. Comparison of numerical results and experimental data.

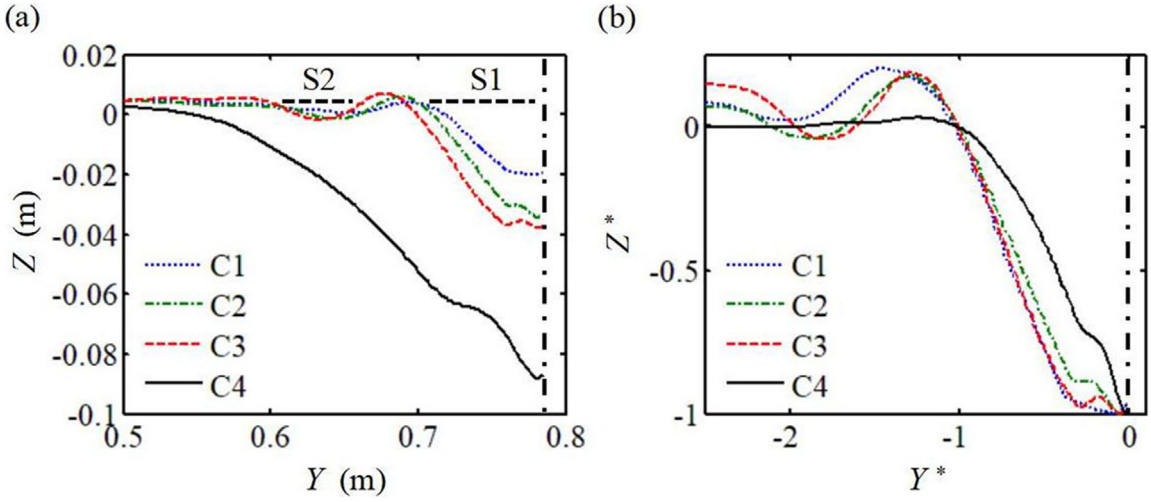

Fig. 5. Topography at $X = 1$ m cross section obtained from the experiments: (a)dimensional topography; and (b) dimensionless topography.

with the experimental data. However, in the downstream region away from spur dike, the fine grid is better than the coarse grid, indicating that the computational accuracy in this region is more sensitive to the grid size. So the fine grid is used in this study for the numerical computation of the rest cases (C1-C3).

The contraction ratio, which is commonly used to describe the flow retarding properties of hydraulic structures in the contraction section of a river channel, is the ratio of river width to spillway area. In Fig. 4, *ABHG* represents the overflow area of the river before it is affected by the spur dike, *ABOC* is the flow retarding area of the dam structure, *COHG* is the overflow area of the contraction section of the river before local scour begins, and *ODF* represents the increase in overflow area caused by the scour hole.

Scouring caused by in-stream structure can be broadly categorized into contraction scour and local scour. Contraction scour is mainly caused by the accelerated water flow exceeding the critical flow velocity and driving sediment movement. Local scour is mainly caused by strong turbulence in the local flow field. In natural rivers, the width *OH* of the constricted section is generally much greater than the width *OF* of the scour hole. Therefore, when evaluating the scour caused by the acceleration of the main flow, the change in overflow area caused by the scour hole can be considered negligible. However, when analyzing the local scour in the vicinity of the spur dike, the change in topography and the increase in flow area caused by the scour hole have a certain impact on the flow field. In particular, the development of the main scour hole near the spur dike head can induce complex vortex-flow evolution phenomena in the local flow field before the water and bed reach a dynamic equilibrium state. In this study, the cross-sectional area fraction of the main scour hole is used to represent the degree of topographic change:

$$\Delta A = \frac{A_{\mathrm{ODF}}}{A_{\mathrm{COFE}}} \times 100\%, \tag{6}$$

where A_{ODF} is the cross-sectional area of the main scour hole at the contraction cross-section and A_{COFE} is the local overflow area above the main scour hole. Detailed geometric information for the main scour hole at the cross-section for the four cases can be found in Table 2.

The topographic changes with time at the contraction cross section ($x = 1$ m) are shown in Fig. 5(a). It can be found that there are two scour holes near the head of the spur dike during the initial scouring stage (C1-C3). The main scour hole (S1) is immediately adjacent to the head of the spur dike, while the secondary scour hole (S2) is located next to S1. The development rate of S1 along the vertical direction *Z* shows a clear attenuation phenomenon, but the lateral development rate maintains relatively stable. S2 reached maximum depth in case C2 and then expanded outwards with S1. Then S2 finally merged into the interior of S1. During the initial scouring stage, the slope of S1 was steeper compared to the equilibrium terrain represented by C4. This can be attributed to the greater capacity of the water flow to transport sand during this period, which allows the sand maintain steeper slope.

Table 2
Geometric index values of the main scour hole in each case.

Case	Max scour (cm)	A_{ODF}(cm^2)	A_{COFE}(cm^2)	ΔA(%)
C1	2.0	8.36	126.49	6.6
C2	3.4	14.02	139.97	10.0
C3	3.8	22.65	170.20	13.3
C4	8.8	101.72	515.13	19.7

The *Z* and *Y* coordinates were normalized using the maximum scour depth (*OD*) and lateral width (*OF*) of S1, respectively, to generate the dimensionless topography shown in Fig. 5(b). Figure 5(b) illustrates that the bed elevation lines in C1, C2, and C3 are highly similar. Zhang et al. [15] got similar conclusions when analyzing the topographic changes caused by spur dike with varying angles of installation. Moreover, after applying the dimensionless transformation, S2 in C1-C3 tends to converge gradually towards S1. This indicates that the lateral growth rate of S2 is lesser compared to S1, which is the primary reason for the subsequent incorporation of S2 into the interior of S1. Developed bed and merging of scour holes brought noticeable variances between the initial scour stage and the equilibrium stage, in terms of geometric characteristics. As a result, the flow fields in the above two stages will not be the same. Thus, analyzing the entire process of local scour is inadequate if it relies solely on the flow field under a single terrain condition. It is crucial to adequately consider the effect of flow field variations on sand transport to improve the current sediment transport models [16] used for predicting the maximum scour depth.

As the flow approaches the spur dike, it is accelerated through a constricted area due to the presence of the spur dike extended form the side channel. Then the flow moves downstream and gradually returns to its original velocity distribution. Figure 6 shows the distribution of the average velocity magnitude at the constricted cross section under different cases. The highest flow velocities are observed near the wall of the spur dike, with velocities decreasing as the flow moves away from the wall. The flow in the scour hole compresses the space of motion of the shear flow in the vicinity of the bed and causes deformation at the bottom of the shear flow layer. There is also an increase in high velocity flow near the bed in sections C1-C3. This region is located between the main horseshoe vortex (HV1) and the bed, suggesting that the HVS could influence local sand transport by generating high velocity flow. Due to the increase in flow velocity and the expansion of the influence

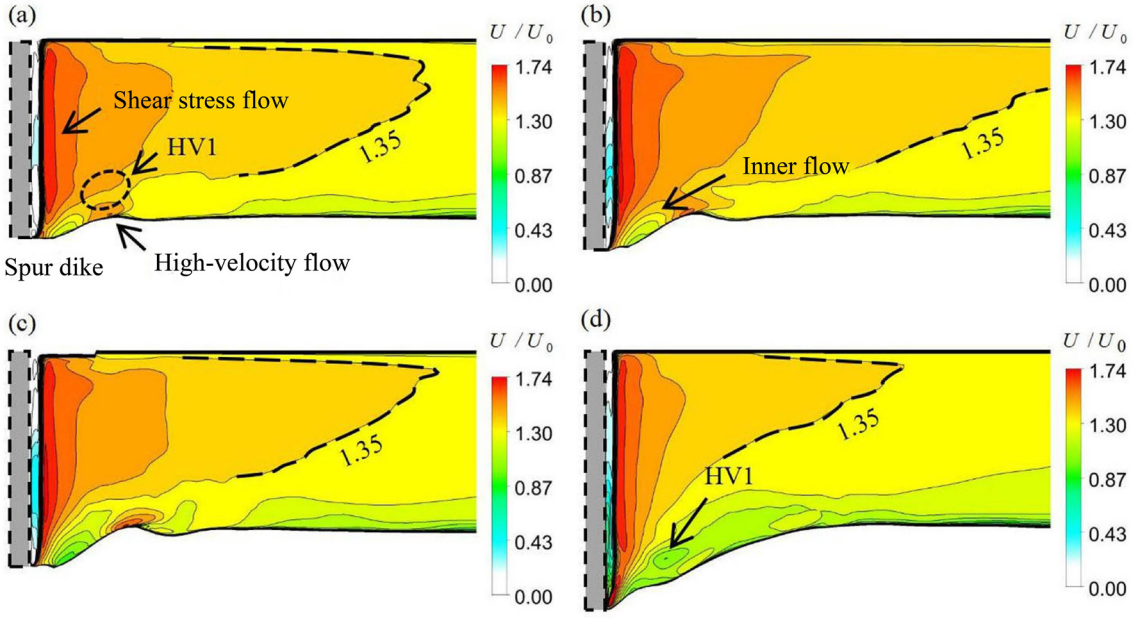

Fig. 6. Velocity contour on $X = 1$ m cross-section: (a) C1, (b) C2, (c) C3, and (d) C4.

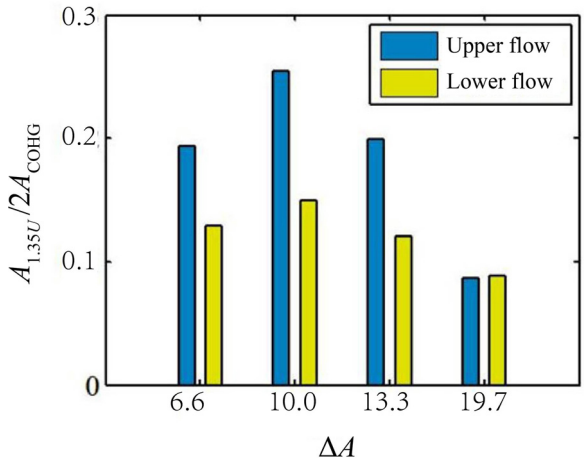

Fig. 7. $A_{1.35U}$ changes with ΔA at $X = 1$ m cross section.

area, the sand transport by the high velocity flow shows a monotonically increasing trend during the initial scour stage. In case C4, the high velocity flow near the wall is significantly attenuated, suggesting that the high velocity flow resulting from the main horseshoe vortex is suppressed and weakened as it sinks into the inner part of the scour hole. Consequently, the amount of sand transport should gradually decreases during this period.

A further noticeable characteristic in Fig. 6 is that the acceleration of the water flow due to the decreased cross-section was greatest at C2 as the scour hole developed. To quantify this feature, the cross section in Fig. 6 has been divided into an upper flow layer ($z > 0.1$ m) and a lower flow layer (0 m $< z < 0.1$ m), and $A_{1.35U}$ was defined as the area whose velocities are higher than $1.35U_0$. Figure 7 presents the variation of the $A_{1.35U}$ occupancy with ΔA in both region. The results show that the presence of scour hole leads to an increase in the area $A_{1.35U}$, which begins to decrease only after C2. This suggests that the change in topography increases the accelerating effect of the deforming bed on the water flow during a certain period. The enhancement effect of the topography only starts to decrease when the scour hole reaches a certain size. Furthermore, when $\Delta A < 10\%$ the acceleration is mainly concentrated in the upper layer, while the acceleration in the lower layer is relatively small. Consequently, the flow acceleration from topography has a limited effect on local scour.

Accelerated flow near the spur dike is one of the important factors causing local scour. Some researchers suggested that the unit width flow rate can reflect the scour capacity of the water flow, so a similar definition, i.e. the unit area flow rate, was used in this study:

$$Q^* = \frac{Q_{S1}}{A_{S1}}, Q_0^* = \frac{Q_0}{A_0}, \tag{7}$$

where A_{S1}, Q_{S1} are the S1 cross-sectional area at $x = 1$ m and the total flow through the cross-section, respectively; A_0, Q_0 are the inlet area and the inlet flow, respectively. It is important to note that the flow field at different cross-sections are not identical. For instance, the scour hole exhibits complex three-dimensional vortex-flow, while the incoming flow at inlet was relatively uniform. Therefore, it is only meaningful to compare Q^* in similar flow regimes. As discussed earlier, the topography of the initial scour stage is very similar, and Fig. 6 also indicates that the flow field inside S1 is approximate. Hence, it is reasonable to use the change of Q^* to represent the variation in scouring capacity of the flow inside S1 at different times during this stage.

It can be found that the total flow rate through the scour hole cross-section consistently increases in Fig. 8(a). This is primarily due to the progressive enlargement of the cross-section area as scouring continues. However, the trend of Q^* with ΔA depicted in Fig. 8(b) demonstrates that although the total flow rate has been increasing, it reaches an extremely high value when $\Delta A = 10\%$. This implies that the scouring capacity of the water flow in S1 is initially enhanced and then weakened. This aligns with the trend and peak moment of $A_{1.35U}$ shown in Fig. 7. It suggests the existence of a positive feedback regulation mechanism between the scour capacity of the water flow near S1 and the topography in the early stage of the initial scouring stage. In other words, the topographic changes caused by the water flow further enhance the scour capacity of the water flow within S1. This mutual enhancement leads to a rapid increase in local sand transport, resulting in a rapid change in topography, as shown by the change in maximum scour depth from C1 to C2 in Fig. 2(a). However, as the scour hole developed to a certain size, subsequent topographic changes begin to weaken the scouring ability of the water flow within S1, brought a negative feedback regulation mechanism. This continues until the water flow is no longer able

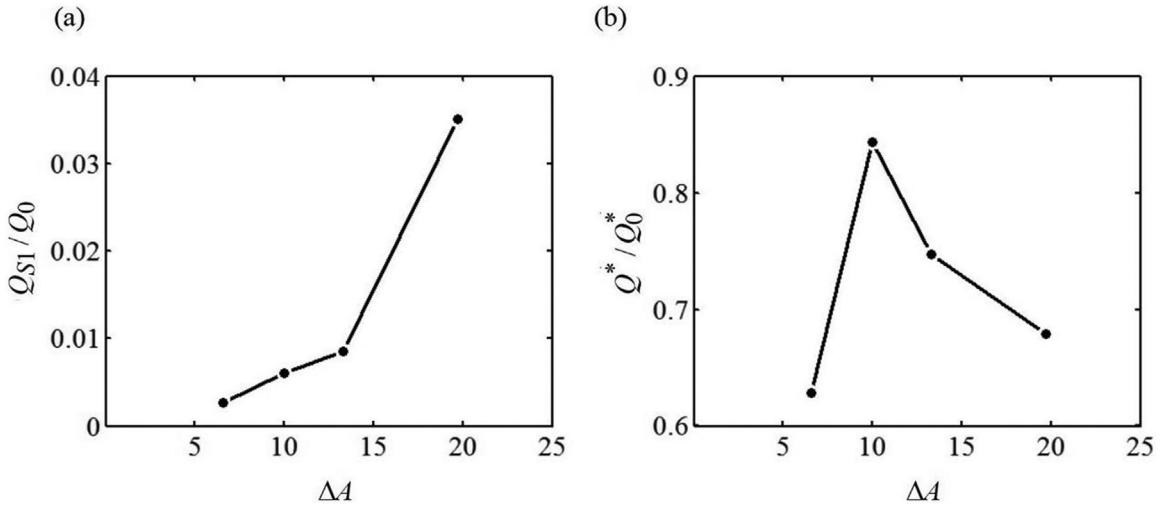

Fig. 8. Flow rate per unit area in the scour hole with ΔA variation.

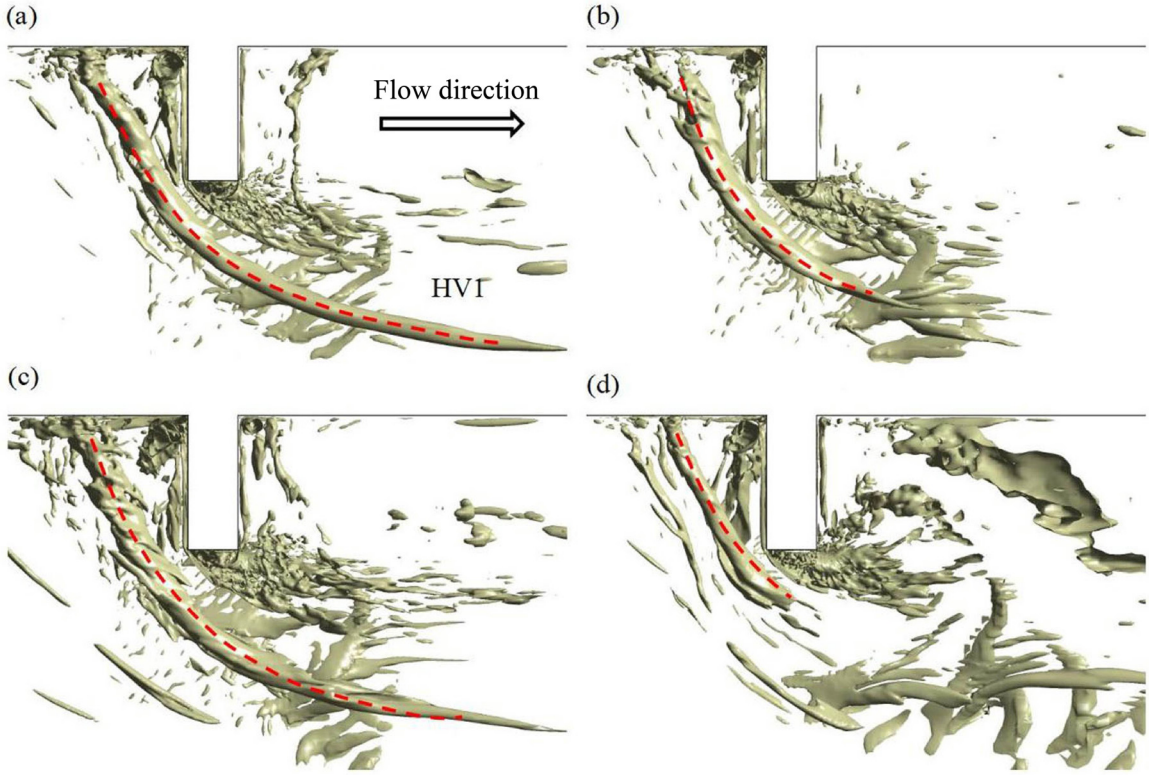

Fig. 9. Vortex structure drawn by isosurface of Rortex=1.5: (a) C1, (b) C2, (c) C3, and (d) C4.

to transport sediment out of the main scour hole. At this moment, the flow field and topography enter a state of dynamic equilibrium.

The horseshoe vortex system moving downstream around the spur dike head near riverbed region is a major factor causing local scour. Figure 9 used Rortex[17,18] to show how the location and range of the primary horseshoe vortex varies with the terrain. It was found that the range of influence of the primary horseshoe vortex was gradually decreasing and the size of the primary horse vortex remains the same. Further more, the horseshoe vortex system located at the contraction cross section in different topographies are shown in Fig. 10. During the initial scour stage (C1-C3), the relative core position of the HV1 vortex did not change significantly and was always located at the junction of S1 and S2. However, the geometry of the vortex core gradually evolved from a circle to a ellipse, which is related to the change in the flow field in the upstream region of the horseshoe vortex system generation. At equilibrium stage, the size of HV1 was drastically reduced, sinking to the bottom of S1. The size and location of the secondary horseshoe vortex (HV2) did not change significantly throughout the scouring process and was only significantly displaced horizontally towards the channel centreline in case C3. This displacement was also closely related to the upstream flow field. In addition, a larger vortex structure formed within S2, located between the main and secondary horseshoe vortices, known as V1. Since the generation of V1 is largely dependent on the local topography, the merging of S2 into S1 in the equilibrium state will lead to the subsequent disappearance of V1.

It can be found from the turbulent kinetic energy (TKE) distribution in Fig. 10 that the instability of the flow in the shear layer due to the high velocity gradient generates a strong TKE area and the rest two

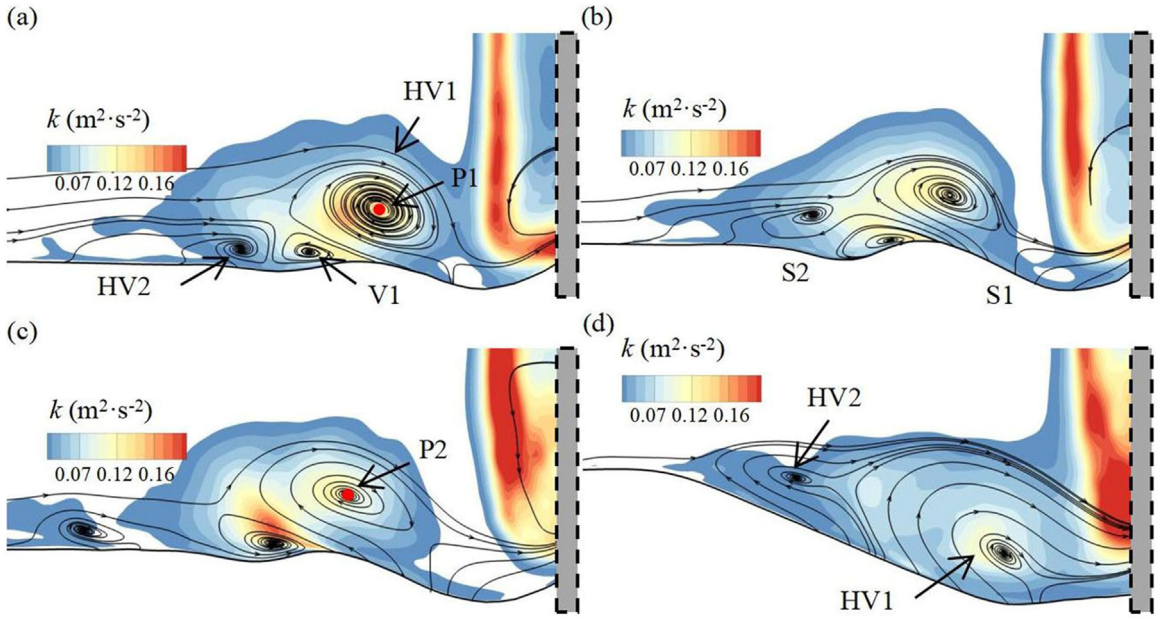

Fig. 10. Streamlines and TKE (k) contour at the contraction cross section: (a) C1, (b) C2, (c) C3, and (d) C4.

Table 3
Comparison of the average non-dimensional time corresponding to successive mode switching.

	Koken 2008	Koken 2009	Case I	Case III
Reynolds number (Re)	1.8×10^4	5.0×10^5	3.1×10^4	3.1×10^4
Topography change (ΔA)	0%	0%	6.6%	13.3%
Average non-dimensional Time (d/U)	3.2	2.8	2.9	2.5

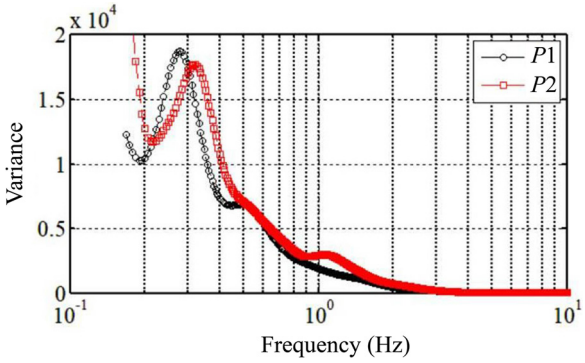

Fig. 11. Wavelet analysis of the streamwise velocity (u) at the core of the HVS.

regions of high TKE area in the flow field are located near HV1. The first one is the interior of HV1 and the turbulent kinetic energy strength in this region tends to gradually decrease with scouring. The second one is located at the junction of HV1 and V1, and the TKE value in this region increases steeply in the C3 condition. Furthermore, it can be seen from Fig. 6 that the water flow velocity in this region also reaches its peak at this time. As the turbulence near the riverbed will entrain sediment particles to the upper flow layer and increase the transport of suspended matter, the main horseshoe vortex in C3 causes the highest sand transport through its own turbulent pulsation. This is an important period for the horseshoe vortex system to influence local scouring.

The existence of the bimodal motion (back-flow and zero-flow) inside the HV1 with flat bed was numerically investigated at two different channel Reynolds number ($Re = 1.8\times10^4, 5.0\times10^5$) by Koken et al. (2008, 2009). Their results pointed out that the average time interval corresponding to successive mode switching inside the HV1 were $3.2d/U$ and $2.8d/U$ for $Re = 1.8\times10^4$ and $Re = 5.0\times10^5$ respectively. And in this study ($Re = 3.1\times10^4$), the similar monitor points P1 and P2 depicted in Fig. 10 were selected for comparison with the results in the above two papers. Then wavelet analysis was used to analyze the average time interval corresponding to successive mode switching inside the bimodal region based on time series of velocity at P1 and P2 obtained by the additional computation (statistics for $60d/U$). The frequency of the min large-scale temporal modulations indicated by peak values in Fig. 11 is about 0.27 Hz ($2.9d/U$) and 0.315 Hz ($2.5d/U$) which is comparable to the value in other researches as shown in Table 3.

A comparison of the data in Table 3 shows that both the increase in Reynolds number and the degree of topography change could reduce the average time interval corresponding to successive mode switching. However, compared to a $0.4d/U$ change in interval time between two modes due to a 30 times increase in Reynolds number, a one times increase in topography change could causes the same magnitude of varies in interval time. It indicates that the bimodal motion of the HVS is more sensitive to topography than the flow Reynolds number.

In summary, this work investigated the evolution of the flow field with the deforming bed and got the following conclusions. The presence of the scour hole in the early stage of initial scour enhances the accelerating effect of the spur dam on the water body. This stage represents a positive feedback control between the scour capacity of the water and topographic changes, and local sand transport increases as scour intensifies. However, as the scour hole grows to a certain size, further topographic changes weaken the sand transport capacity of the water flow, eventually reaching a scour equilibrium state. In addition, the main horseshoe vortex influences local sand transport by generating high velocity flows at the edge of the scour hole close to the river bed near the head of the spur dike. In the later phase of the initial scour stage, the localised eddy structure in the second scour hole, combined with the main horseshoe eddy, significantly increases the turbulence energy at their junction position, further enhancing the transport of suspended sediment. Therefore, the influence of the main horseshoe vortex on local scouring reaches its maximum effect after the scouring process has been underway for a certain time.

It is important to note that this study is based on experimental and numerical results for a specific scour condition, so the changes in the flow field during local scour requires further research. However, the present results show that the bimodal motion within the HVS was sensitive to the topography, then the influence of the topography on the flow field and the sand transport capacity of the water flow cannot be overlooked. In future work, it is crucial to conduct more comprehensive scour experiments to investigate the feedback regulation mechanism between the flow and bed in order to improve our understanding of local scour.

Declaration of competing interest

The authors declare that they have no known competing financial interests or personal relationships that could have appeared to influence the work reported in this paper.

Acknowledgments

This work was supported by Shenzhen Science and Technology Program (Grant No. JCYJ20220818102012024) and Hong Kong Research Grants Council (Grant Nos. T21–602/16-R and RGC R5037–18).

References

[1] B Przedwojski, Bed topography and local scour in rivers with banks protected by Groynes, J. Hydraulic Res. 33 (2) (1995) 257–273.
[2] B.S. Wu, G.Q. Wang, J.M. Ma, R Zhang, Case study: river training and its effects on fluvial processes in the lower Yellow River, China, J. Hydraul. Eng. 131 (2) (2005) 85–96.
[3] H. Azinfar, J.A Kells, Drag force and associated backwater effect due to an open channel spur dike field, J. Hydraulic Res. 49 (2) (2011) 248–256.
[4] P.M. Biron, C. Robson, M.F. Lapointe, S.J Gaskin, Three-dimensional flow dynamics around deflectors, River Res. Appl. 21 (9) (2005) 961–975.
[5] H. Aung, B. Onorati, G. Oliveto, G Yu, Riverbed morphologies induced by local scour processes at single spur dike and spur dikes in cascade, Water (Basel) 15 (9) (2023) 1746.
[6] N.S. Cheng, Y.M Chiew, Incipient sediment motion with upward seepage, J. Hydraulic Res. IAHR 37 (5) (1999) 665–681.
[7] S.Q Yang, Formula for sediment transport subject to vertical flows, J. Hydraul. Eng. 145 (5) (2019) 04019013.1-04019013.11.
[8] S.T. Tsai, Sedimentation motion of sand particles in moving water (I): the resistance on a small sphere moving in non-uniform flow, Theor. Appl. Mech. Lett. 12 (6) (2022) 100392.
[9] M.Y.G Iman, D.B. Brian, Experimental study on particle pick-up rate of vertical vortices, J. Hydraul. Eng. 147 (4) (2021) 06021003.
[10] M. Koken, G Constantinescu, Flow and turbulence structure around a spur dike in a channel with a large scour hole, Water Resour. Res. 47 (12) (2011).
[11] J. Unger, W.H Hager, Down-flow and horseshoe vortex characteristics of sediment embedded bridge piers, Exp. Fluids 42 (1) (2007) 1–19.
[12] D.W. Guan, Y.M. Chiew, M.X. Wei, S.C Hsieh, Characterization of horseshoe vortex in a developing scour hole at a cylindrical bridge pier, Int. J. Sediment Res. 34 (2) (2019) 118–124.
[13] J.H. Si, S.Y. Lim, X.K Wang, Evolution of flow fields in a developing local scour hole formed by a submerged wall jet, J. Hydraul. Eng. 146 (6) (2020) 04020040.
[14] D.K. Lilly, A proposed modification of the Germano subgrid-scale closure method, Phys. Fluids A 4 (3) (1992) 633–635.
[15] L. Zhang, H. Wang, X.Q. Zhang, B. Wang, J Chen, The 3-D morphology evolution of spur dike scour under clear-water scour conditions, Water (Basel) 10 (11) (2018) 1583.
[16] M.A. Zhao, Review on recent development of numerical modelling of local scour around hydraulic and marine structures, J. Mar. Sci. Eng. 10 (8) (2022) 1139.
[17] J.M. Zhan, Y.T. LI, W-H.O. Wai, W.Q Hu, Comparison between the Q criterion and Rortex in the application of an in-stream structure, Phys. Fluids 31 (12) (2019) 121701.
[18] Y.T. Li, W-H.O. Wai, J.M. Zhan, W.Q. Hu, X.F. Yan, Evolution of three-dimensional flow field and vortex structures around a single spur dike during the scouring process, J. Hydraul. Eng. 150 (1) (2024) 04023057.